

Multiple-level Logarithmic Wavelets for Mammographic Contrast Enhancement: A Statistical Analysis for Wavelet Selection

Damian Valdés Santiago¹, Daniel Mesejo León², Ángela León Mecías¹

¹ Universidad de La Habana, Facultad de Matemática y Computación,
Departamento de Matemática Aplicada,
Cuba

² Pontifical Catholic University of Rio de Janeiro,
Brazil

dvs89cs@gmail.com, dmesejo@gmail.com, angela@matcom.uh.cu

Abstract. Low doses radiation in mammography results in low contrast images. In this paper we propose a method to enhance the contrast in mammography; it combines the modification of the coefficients of the Logarithmic Discrete Wavelet Transform using the Local Correlation method and Symmetric Logarithmic Image Processing model. Experimental results shown the better performance for the anomalies known as calcifications and masses. This paper also presents a methodology to select a combination of decomposition levels to be processed for good contrast improvement according to the values of measures based on region of interest. This procedure relies on Principal Components Analysis of the data. The experiments show that the chosen combination of levels can improve the contrast in mammograms, and that the regions of interest definition is an important factor to explain the poor contrast improvement of some anomalies.

Keywords. Mammograms, contrast enhancement, discrete wavelet transform, symmetric logarithmic image processing model, logarithmic discrete wavelet transform.

1 Introduction

Breast cancer screening is the medical procedure of asymptomatic, apparently healthy women in an attempt to achieve an earlier diagnosis [36]. Mammography is the most common screening method since it is relative fast, cheap and widely available. This imaging process use a very low ionizing radiation dose to examine the human

breast, due to the resulting image has low contrast and the different parts of the breast are hard to distinguish, in particular, detecting masses and microcalcifications requires years of medical training. The anomalies vary in size and shape, and might be located in dense tissues making their detection more difficult. Also, breast tissues are different in younger and senior women [18]. Conventional methods like CLAHE, Unsharp Masking, median filtering and Gaussian filtering don't have enough visual quality to help a radiologist [1].

The wavelets approach has been widely used in digital mammography with satisfactory results [1]. Nevertheless, there are few works that establish a procedure to choose the wavelet base and the combination of decomposition levels that must be processed to effectively increase the contrast in mammographies [5]. This paper proposes a methodology to select the decomposition levels to be process in wavelet-based algorithms. A contrast improvement is performed by modifying the wavelet coefficients using the Local Correlation method in a logarithmic framework [4, 22]. Quantitative contrast measures [34] and Principal Components Analysis [15] are used to select the best combination of decomposition levels.

The rest of the paper is structured as follows. Section 2, introduce the Discrete Wavelet Transform and the Logarithmic Image Processing framework. In Section 3, we

propose an algorithm based on the Logarithmic Discrete Wavelet Transform for mammography contrast enhancement. In Section 4 we present a methodology to select wavelet base and combination of decomposition levels to be processed for a good contrast enhancement of breast anomalies. The experimental setup is described in Section 5. In Section 6, the results are discussed. Some remarks and conclusion are given in Section 7.

2 Discrete Wavelet Transform and the Logarithmic Image Processing Framework

A gray-level image is a function $f : D \subset \mathbb{R}^2 \rightarrow [0, M] \subset \mathbb{R}$. The mammography images used in the experiments have 12 bits of gray levels, so $M = 4096$.

The Discrete Wavelet Transform (DWT), derives from the discretization of the scaling factor a (dilation or contraction) and the translation (or localization), parameter b in the mother wavelet:

$$\begin{aligned}\zeta_{j,k}(x) &= 2^{-j/2} \zeta(2^{-j}x - k), \\ &= \frac{1}{\sqrt{2^j}} \zeta\left(\frac{x - 2^j k}{2^j}\right), (j, k) \in \mathbb{Z}^2.\end{aligned}\quad (1)$$

A discrete scaling function φ is associated with the considered mother wavelet ζ :

$$\begin{aligned}\varphi_{j,k}(x) &= 2^{-j/2} \varphi_0(2^{-j}x - k), \\ \zeta_{j,k}(x) &= 2^{-j/2} \zeta_0(2^{-j}x - k), k \in \mathbb{Z},\end{aligned}\quad (2)$$

with these two functions constituting a Riesz basis [25].

The computation of the DWT can be expressed by the approximation coefficients WT_φ and the detail wavelet coefficients WT_ζ [12]:

$$\begin{aligned}WT_\varphi(j_0, k) &= \langle f, \varphi_{j_0, k} \rangle, \\ WT_\zeta(j, k) &= \langle f, \zeta_{j, k} \rangle,\end{aligned}\quad (3)$$

with $j_0 \leq j$, ζ is the mother wavelet and φ the scaling function.

φ and ζ generate an orthonormal basis of $L^2(\mathbb{R})$. Three directional wavelets are obtained

by the product of a 1-D scaling function and the corresponding wavelet function:

$$\begin{aligned}\zeta^H(x, y) &= \varphi(x)\zeta(y), \\ \zeta^V(x, y) &= \zeta(x)\varphi(y), \\ \zeta^D(x, y) &= \zeta(x)\zeta(y),\end{aligned}\quad (4)$$

$\zeta^i, i \in \{H, V, D\}$ allows the detection of horizontal, vertical and diagonal variations in the image.

According to Mallat [21], the 2-D wavelet is defined as:

$$\zeta_{j,k}^i(x, y) = 2^j 2^i \zeta^i(2^j x - k_1, 2^j y - k_2). \quad (5)$$

The whole image $f(x, y)$ decomposes as:

$$\begin{aligned}f(x, y) &= \sum_{j,k,i} d_{j,k}^i 2^j \zeta_{j,k}^i(x, y), \\ d_{j,k}^i &= \langle \zeta_{j,k}^i, f(x, y) \rangle.\end{aligned}\quad (6)$$

The DWT provides a ‘measure of similarity’ between the image and the mother wavelet around the pixel (x, y) , at the given scale. It means that if the image is constant or do not vary ‘too much’ in the support of a wavelet, then its wavelet transform will be zero or very small, this is how wavelets provide information about the local contrast of an image [28]. This fact is useful because anomalies can be detected with the detail coefficients and can be isolated to improve the contrast against the surrounding region [22, 19, 28].

Generally, the wavelet-based algorithms have three main stages. First, the image is decomposed in horizontal, vertical and diagonal detail coefficients and the approximation coefficients. At this stage is important to select the wavelet base and levels of decomposition to be process. Different approaches for wavelet base selection has been addresses in [29, 11]. Cheng et al. proposed an automatic wavelet base selection to enhance contrast of natural images [5]. In this contribution we study a way to select the proper wavelet base to improve contrast in mammography images, also related with the type of anomaly; to our knowledge this task hasn’t been done yet.

Usually, in the literature all decomposition levels are processed until a selected one (each wavelet base have a maximum level of decomposition).

A low decomposition level implies more efficiency of the wavelet decomposition algorithm. In previous work we founded that its not necessary to process all the levels to enhance the contrast [37]. Due to, in our proposal we include a methodology to select levels of decomposition to be process. In our bibliography study we don't find evidence of similar approach.

In the second stage of wavelet-based algorithms, the detail coefficients of selected decomposition levels are modified to improve the contrast. Finally, applying the inverse wavelet transform (IDWT), the enhanced image is obtained.

There are several methods for modifying the detail coefficients. A group of algorithms uses a non-linear function that follows certain criteria established by Laine and Song [20]. Some methods apply heuristics over the wavelets coefficients, e.g. Simple, Threshold, Correlation and Local Correlation methods [22]. In [37] we demonstrated that the most effective method is the Local Correlation. It is based on the following theoretical concept: coefficients that retain high values at different decomposition levels must be correlated and therefore are part of an anomaly. For detecting high values are only considered the coefficients of a neighborhood, hence the name local. This concept was presented by Stefanou et al. [35] and Chen et al. [4]. This method achieves a good increment of the contrast of the masses and other elements such as the pectoral and the edge of the breast.

2.1 Non-Linear Models for Image Processing

The non-linear models of image processing (NIP, also known as Logarithmic Models), are an alternative to the classical image processing, based on floating-point arithmetic, because this approach has the limitation of truncating the sum of pixel values over the limit. These NIP models modify the basic operations over the pixel intensities. The superiority against classical methods has been proved in [10, 17].

NIP models represent an image using an algebraic structure, so it performs operations different to the classical ones (point-to-point).

The mathematical construction of a NIP model starts by the definition of the operational laws (addition and multiplication by scalar), or equivalently finding a generating function (isomorphism), that represents the definition of the model in a real algebraic structure [10]. What distinguishes the models is the isomorphism, since it determines the operations of the algebraic structure. There are several NIP models, but in the experimentation performed in this contribution the S-LIP model [26] was used.

2.1.1 Symmetric Logarithmic Image Processing Model

The Symmetric Logarithmic Image Processing Model (S-LIP), was proposed by Navarro et al. [26] to overcome the disadvantages of previous models with respect to symmetry and its visual meaning.

This model defines the following isomorphism $\Phi : (-M, M) \rightarrow (-\infty, \infty)$:

$$\Phi(u) = -M \operatorname{sgn}(u) \ln \left(\frac{M - |u|}{M} \right), \quad (7)$$

with the inverse:

$$\Phi^{-1}(u) = M \operatorname{sgn}(u) \left(1 - e^{-\frac{|u|}{M}} \right), \quad (8)$$

Φ its necessary to apply traditional tools like Fourier transform and wavelet transform [17].

Navarro et al. use the Logarithmic Discrete Wavelet Transform (LDWT), and S-LIP model in compression, edge detection and noise suppression in images [25].

3 Logarithmic Discrete Wavelet Transform for Contrast Enhancement in Mammography

The logarithmic wavelet was introduced by Courbebaisse et al. in 2002 [6]. In their paper they prove the advantages of using this type of wavelet to solve problems like detection of singularities. The idea behind logarithmic wavelets is to dilate and translate a wavelet function in a non-linear way. This kind of wavelets are superior to the classic ones because their amplitude changes logarithmically and remain bounded [25].

The S-LIP mother wavelet ζ_{Δ} associated with the linear mother wavelet ζ is defined as [25]:

$$\zeta_{\Delta} = \Phi^{-1}(\zeta), \quad (9)$$

where Φ is the isomorphism of S-LIP model.

Then,

$$\zeta_{\Delta}(a, b)(x) = \frac{1}{\sqrt{a}} \Delta \left(\zeta \left(\frac{x-b}{a} \right) \right), \quad (10)$$

where Δ is the scalar product defined by the isomorphism of S-LIP model.

The three directional S-LIP wavelet are defined as:

$$\begin{aligned} \zeta_{\Delta}^H(x, y) &= \varphi_{\Delta}(x) \Delta \zeta_{\Delta}(y), \\ \zeta_{\Delta}^V(x, y) &= \zeta_{\Delta}(x) \Delta \varphi(y), \\ \zeta_{\Delta}^D(x, y) &= \zeta_{\Delta}(x) \Delta \zeta_{\Delta}(y). \end{aligned} \quad (11)$$

The logarithmic wavelet decomposition of image f is:

$$\begin{aligned} f(x, y) &= \sum_{i,j,k,n}^{\Delta} d_{j,m,n}^i 2^j \Delta \zeta_{\Delta j,m,n}^i(x, y), \\ d_{j,m,n}^i &= \langle \zeta_{\Delta j,m,n}^i, f(x, y) \rangle_{\Delta}. \end{aligned} \quad (12)$$

The scalar product in S-LIP model is defined as:

$$\langle f, g \rangle_{\Delta} = \sum_{i=1,2,\dots,n}^{\Delta} f_i g_i. \quad (13)$$

As we present, the LDWT can be defined using the non-linear operations of the model, however we used another approach. This approach consists in apply Φ to the image, calculate the DWT and afterward reverse the transformation using Φ^{-1} . The main difference between both ways is the computational cost of the isomorphism [25, 17].

The algorithm proposed in our contribution uses LDWT in a S-LIP model and achieve contrast enhancement through modifying wavelet coefficients with Local Correlation method, as shown in Figure 1.

4 Statistical Analysis for Wavelet Selection

In this section we propose a methodology for wavelet selection, i.e. select the wavelet base and the combination of decomposition levels to be processed. This approach needs the wavelet decomposition of an image for a set of wavelet bases and all possible combinations of decomposition levels, i.e. the power set of $\{1, 2, 3, \text{maximum level of decomposition}-1\}$. Then, a modification of wavelets coefficients is performed in order to increase the contrast. Finally, we obtain the reconstructed image through IDWT, and a quantitative quality measure is computed on it.

The experimentation presented in this research apply LDWT with S-LIP, model to an image up to the highest decomposition level using a set of wavelet bases. After that, modify the wavelet coefficients by means of the Local Correlation method. Contrast enhancement quality measures based on regions of interest are computed for all the anomalies present in the image.

According to the type of anomaly the best wavelet base was selected following different points of view namely: quality measure, descriptive statistics, visual results, and experiences on wavelet selection presented in reviewed bibliography.

Having the best wavelet base, we choose the decomposition level to be processed through a Principal Components Analysis (PCA) [15], performed to the data fetched from each basis where each column is a different combination of decomposition levels and each row represents the value of the quality measure matching each represented reconstructed image.

PCA reduces the data dimension based on the data variance allowing the visualization of high dimensional data, correlated variables, and more significant variables for describing data. This technique center data with respect to the data mean and then calculates the co-variance matrix [15].

PCA allows us to do the *loadings* plot where the variance of each combination of decomposition levels is shown. The interpretation of this plot enable to know the behavior of level combinations for contrast enhancement.

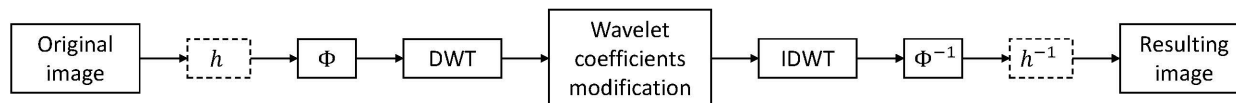


Fig. 1. Proposed algorithm for mammography contrast enhancement

The module of *loadings* vectors represents the deviation of each combination with respect to the data mean. The cosine of the angle between these vectors denote the correlation between the variables that its characterize. An angle near to 0° or 180° means co-linearity (redundancy), whilst an amplitude of 90° and 270° degrees imply low correlation.

The Manhattan plot [7], is another way to interpret the variance of each level combination and complements the results of the *loadings* plot. This plot consists on a grid which rows are the principal components considered and the columns are the variables of the model (combinations of decomposition levels in this paper). Each cell of the grid have a gray intensity corresponding to explained variance of each variable in the selected component. The black color means 0% explained variance and white represents 100% [31].

We considered the two principal components if these components captures more than 50% of the data variability. Then, we get the combinations that capture more than 90% of the variability per each reconstructed image in the first principal component.

A combination of levels is called “suitable” if it displays the highest variance, the lowest feasible level and the fewest amount of levels to be processed. This criterion is justified because wavelet transform is more efficient if the decomposition is performed to a low level [21]. The obtained combination of decomposition levels allow us to achieve the best contrast improvement according to the quantitative quality measure used.

5 Experimental Setup

The algorithm was tested on 94 sub-images of the image 22670465 of INbreast data set [23]. This image was selected because it contains most diverse set of anomalies of the data set (one

mass, one spiculated region, one cluster and 92 calcifications). In this image, anomalies called asymmetry and distortion are not present.

In the used data set each anomaly is annotated using a contour for masses and calcifications and a circle for spiculated regions and clusters.

5.1 Contrast Enhancement Quality Measures

A region of interest (ROI), is formed by a foreground that contains the anomaly, and the background that comprises the surrounding tissue. This construction reflects human visual perception as it perceives an object considering the environment where it is placed. The ROI's based measures quantifies the contrast of a mammogram's region chosen by the radiologist or defined automatically.

The INbreast's contours by anomaly was considered as ROI's foreground. Since a ROI can vary in forms and size, a flexible background contour is needed. The adaptive margin for this contour was calculated according to the algorithm proposed by Mudigonda et al. [24].

In this paper, the contrast enhancement quality was quantified using Contrast Improvement Index (CII) [30] and Combined Enhancement Measure (CEM) [34]:

$$CII = \frac{C_{processed}}{C_{original}}, \quad C = \frac{f - b}{f + b}. \quad (14)$$

CII capture the gain of contrast between original and processed images, it is always positive, and values greater than the unit are considered like a sign of good contrast improvement [32, 30].

CEM combine other three measures: Distribution Separation Measure (DSM), Target-to-Background Contrast Enhancement Measurement Based on Standard Deviation (TBC_s),

and Target-to-Background Contrast Enhancement Measurement Based on Entropy (TBC_ε):

$$CEM = \sqrt{(1 - DSM)^2 + (1 - TBC_s)^2 + (1 - TBC_\varepsilon)^2}, \quad (15)$$

$$DSM = \left| \mu_F^E - \mu_B^E \right| - \left| \mu_F^O - \mu_B^O \right|, \quad (16)$$

$$TBC_s = \frac{\left(\frac{\mu_T^E}{\mu_B^E} \right) - \left(\frac{\mu_T^O}{\mu_B^O} \right)}{\frac{\sigma_T^E}{\sigma_T^O}}, \quad (17)$$

$$TBC_\varepsilon = \frac{\left(\frac{\mu_T^E}{\mu_B^E} \right) - \left(\frac{\mu_T^O}{\mu_B^O} \right)}{\frac{\varepsilon_T^E}{\varepsilon_T^O}}. \quad (18)$$

DSM quantifies the overlapping between the anomaly and the surrounding tissue, TBC_s computes the contrast gain through standard deviation and the mean value of intensities in foreground, before and after the application of the method; and TBC_ε calculated the ROI's homogeneity with entropy [34]. Decrease in CEM marks the improvement in sharpness and edge strength [2, 13].

5.2 Software and Hardware

The algorithms in this work were implemented using Python 2.7.6 programming language [39]. Also we used the modules PyWavelets 0.2.2 [42], NumPy 1.7.1 [41], SciPy 0.13.0 [16], Matplotlib 1.3.1 [14], skimage 0.9.3 [38], sklearn 0.14.1 [27] and OpenCV 2.4.6.0 [3].

6 Results and Discussion

The experimentation was split up in the following steps. First, we apply LDWT with S-LIP model to the image up to the highest decomposition level using the following wavelet bases considered in PyWavelets [42]: Haar, Daubechies 1-20, Symlets 1-20, Coiflets 1-5, Biorthogonal 1.1-6.8, Reverse Biorthogonal 1.1-6.8 and Meyer. After that, we modified the wavelet coefficients by means of the Local Correlation method for all possible combinations of decomposition levels. CII and CEM quality measures are computed for all the ROIs presents in the image.

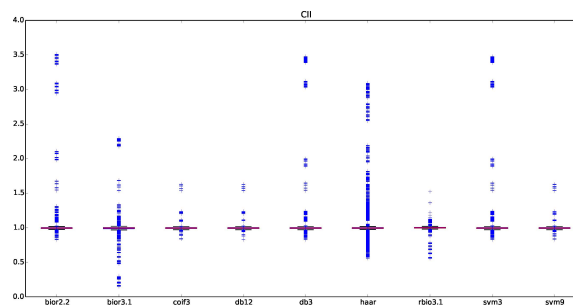


Fig. 2. Boxplot of the CII measure values for a group of wavelet bases

The behavior of the CII measure in the quality of the image contrast enhancement obtained by different wavelet bases shown low dispersion with respect to the central value 1.0. Although, we observed different behaviors for different type of anomalies (in parentheses we put the values of the measure): for the masses a meaningful contrast enhancement was achieved by the wavelet bases Biorthogonal 2.2 (3.51), Daubechies 3 (3.48) and Symlets 3 (3.48) and for spiculated regions and calcifications the worst results are attained by the Biorthogonal 3.1 (0.14), Reverse Biorthogonal 3.1 (0.55) and Haar (0.55) bases. Also, with this measure we obtained similar behavior for a group of wavelet bases, e.g. in a first group the bases Coiflet 3, Coiflet 4, Coiflet 5 and Meyer; in a second group the bases Daubechies 10-20; and in a third group the bases Symlets 7-20.

In Figure 2, the behavior of some selected wavelet bases is shown, and in Figure 3 we illustrate the ROIs of the three best and worst results of the measure CII with the corresponding wavelet bases and decomposition levels.

The CEM measure gives better results when their values are positive and close to zero. Very poor results are obtained for the wavelet bases Reverse Biorthogonal 1.1 (33.53), Haar (33.46) and Biorthogonal 1.1 (33.42). The best contrast increments for this measure were achieved for the bases Reverse Biorthogonal 3.3 (1.33), Biorthogonal 3.1 (1.33) and Biorthogonal 2.2 (1.34).

In this case we also observed a similar behavior for group of wavelet bases, e.g. Coiflet 3, Coiflet

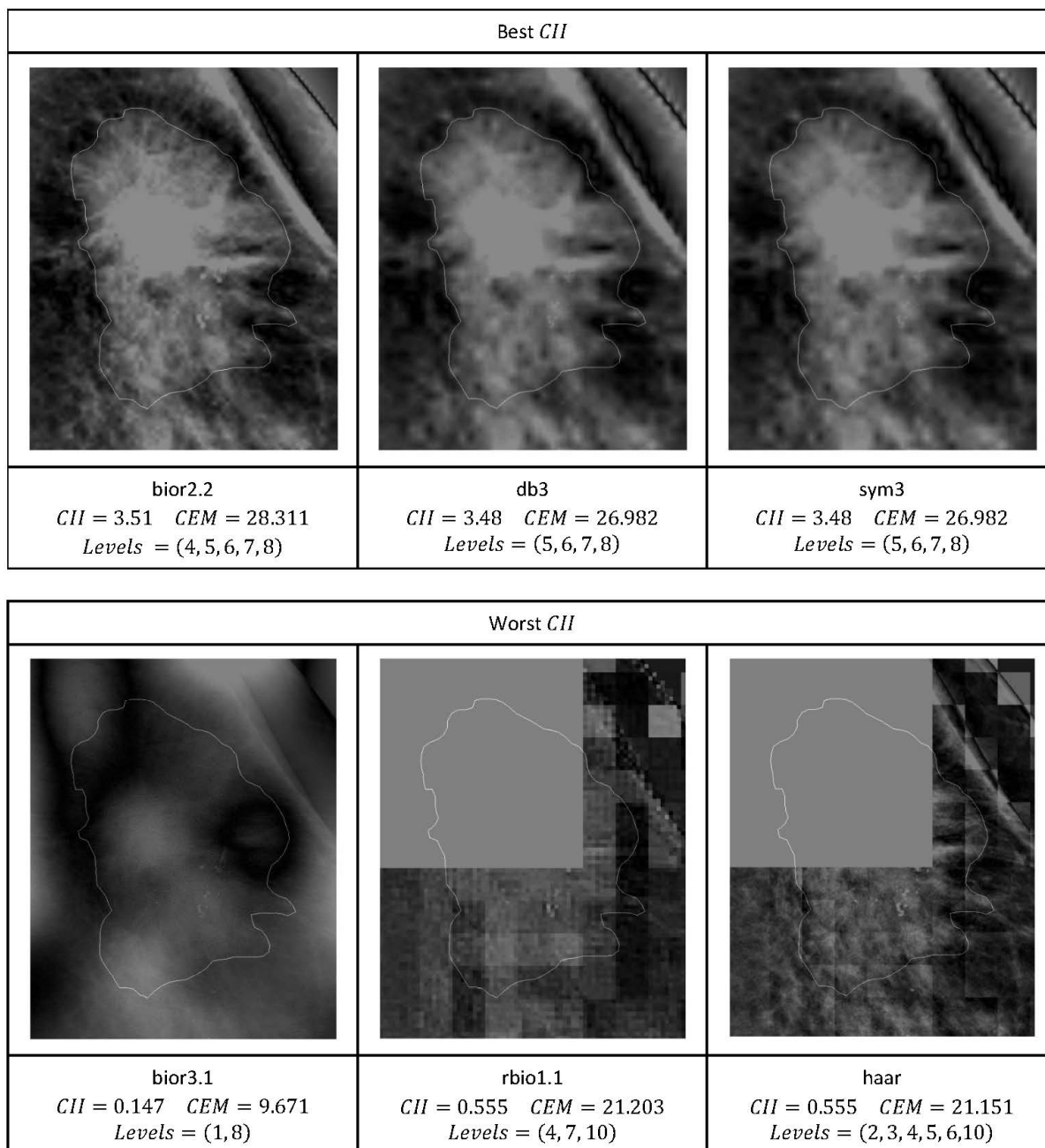


Fig. 3. Best and worst values of *CII* measure with the corresponding wavelet basis

4, Coiflet 5 and Meyer in a first group; Daubechies 10-20 in a second group; and Symlets 7-20 in a third group.

In Figure 4 we illustrate the behavior of the measure *CEM* for a selected group of wavelet bases. In Figure 5, ROIs of the three best and

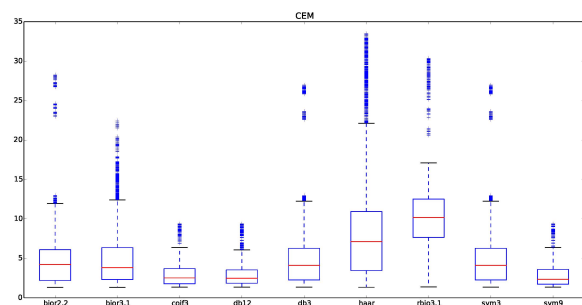


Fig. 4. Boxplot of the *CEM* measure values for a selected group of wavelet bases

three worst results of the measure *CEM* with the corresponding wavelet bases and decomposition levels are shown.

We calculated the average of the measures *CII* and *CEM* for each anomaly and for each wavelet base. Putting all this curves together we can observe the behavior of a specific wavelet base regarding all type of anomalies, as you can see in Figures 6, 7 and 8.

With respect to measure *CII*, the contrast enhancement for the calcifications was poor on average, See Figure 6. For the masses, the contrast was always increased except for the Reverse Biorthogonal 3.1, in fact this was the type of anomaly with higher values for the measure. For the cluster anomaly, the higher contrast enhancement were scored by wavelet bases Biorthogonal 1.3, Biorthogonal 3.1 and Reverse Biorthogonal 1.3, and the worst results were obtained by Biorthogonal 1.1, Haar and Reverse Biorthogonal 1.1. In the case of the spiculated regions, the best values for this measure were achieved with the Biorthogonal 1.1, Daubechies 1 and Reverse Biorthogonal 1.1 bases, reaching its lower value for the Biorthogonal 3.1 basis (See Figure 7).

In Figures 9 and 10 we show in the diagonal the ROIs, for each type of considered anomaly, processed by the wavelet base which produce the best contrast enhancement according to quality measures *CII* and *CEM*, respectively. In each row of both figures the same ROI is processed by the wavelet bases used successfully for the rest of the anomalies. This way we can know if we get, with

the same wavelet base, good results to different anomalies.

Although, the visual results do not match the successful values of the quality measures, Figure 11 shows a selection of good visual results for a ROI corresponding to each one of the four types of analyzed anomalies.

In Figure 12, as you can observe we have markers with different shapes, indicating the wavelet base and different colors for each type of anomaly. The horizontal axis refer to the values of the *CII* measure and the vertical one denote the values of the *CEM* measure. The optimal location in this graphic would be as close as possible to the horizontal axis and as far as possible to the vertical axis, which means small values of *CEM* and large values of *CII*. As it can be seen, the points are far from this region. The best values are below $CEM = 7$ and $1.0 < CII < 2.5$. On this zone mass anomalies stand out for the Symlets 12, Reverse Biorthogonal 3.3, Biorthogonal 1.1, Reverse Biorthogonal 1.3 and Biorthogonal 2.2 bases. Only for the mass anomalies the results of the measures match the visual results.

The quality measures for the enhancement do not provide enough information on their own for the best base selection for improving the contrast. According to research in the literature, Drukker et al. [9] used Biorthogonal 6.8 and Bhateja & Devi [1] uses the Daubechies 6 wavelet basis for the detection of microcalcifications on mammography images. Our experimentation shows that the average value of the *CII* measure for this wavelet basis isn't good, nevertheless the value of the *CEM* measure is low. Visual results confirm the effectiveness of the basis for increasing the contrast on this kind of anomaly. Zhuangzhi et al. presented an Approximation Weighted Detail Contrast Enhancement (AWDCE) filter [43] for detecting masses by the Daubechies 20 wavelet base. However, no well defined analytic approach has been applied for determination of the level of decomposition using Daubechies 20. Schebesch et al. [33] and Vikhe and Thool [40] used Haar basis for detection of masses. Zanchetta et al. used the Daubechies 8, Symlet 8 and Biorthogonal 3.7 bases for classifying masses in normal or abnormal through supervised learning, achieving

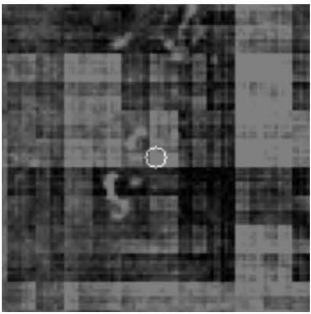
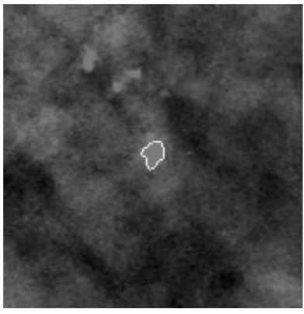

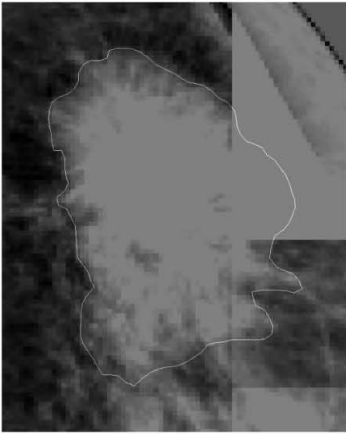
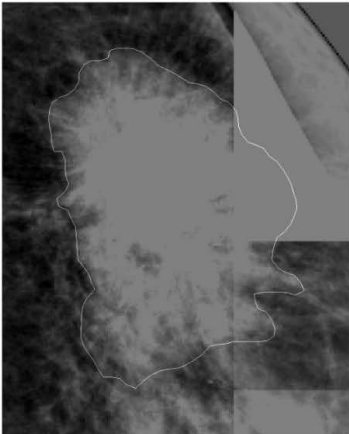
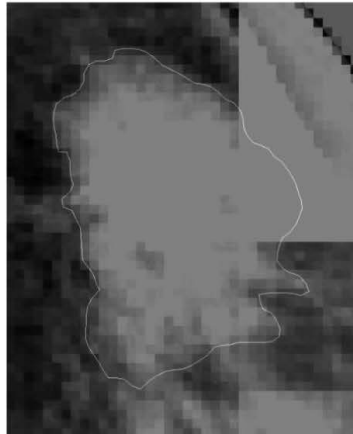
Best <i>CEM</i>		
		
rbio3.3 $CII = 0.949$ $CEM = 1.332$ Levels = (2, 3, 4, 6, 7)	bior3.1 $CII = 0.947$ $CEM = 1.339$ Levels = (1, 2, 4, 5, 6)	bior2.2 $CII = 0.902$ $CEM = 1.34$ Levels = (4, 7, 8)
Worst <i>CEM</i>		
		
bior1.1 $CII = 3.071$ $CEM = 33.536$ Levels = (4, 5, 6, 7, 8, 9)	haar $CII = 3.07$ $CEM = 33.461$ Levels = (3, 4, 5, 6, 7, 8, 9)	rbio1.1 $CII = 3.057$ $CEM = 33.427$ Levels = (5, 6, 7, 8, 9)

Fig. 5. Best and worst values of *CEM* and the corresponding wavelet base

the best results with Biorthogonal 3.7 [8]. In our experimentation, this basis give the best results for the mass: on average, the values of the *CII* are higher than the unit and the values of the *CEM* measure are close to 7. The visual results of the enhancement are successful. Cheng et al. used wavelet bases Symlets 4, Symlets 9, Symlets

12 and Symlets 20 for increasing the contrast of natural images [5]. All these bases display good results visually, the values of the measures are similar and satisfactory. Except for the work of Cheng et al., the choice of these bases is empirical and doesn't provide any statistical information that compares a choice with a greater number of bases

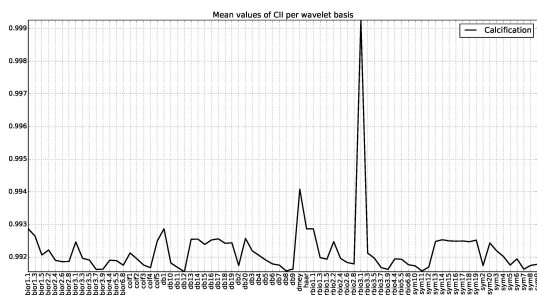


Fig. 6. Mean values of *CII* measure for calcifications and all wavelet families used

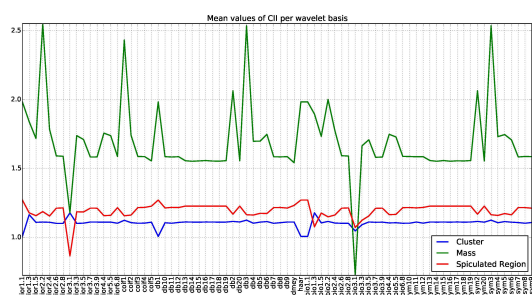


Fig. 7. Mean values of *CII* measure for all type of anomalies and all wavelet families used

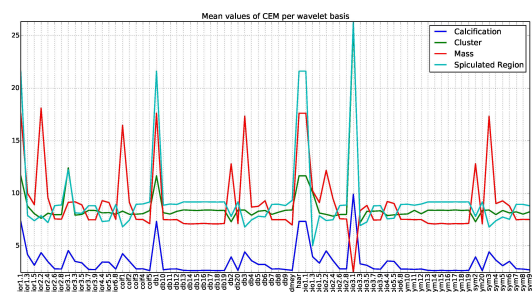


Fig. 8. Mean values of *CEM* measure for all type of anomalies and all wavelet families used

nor a methodology is provided to pick up the decomposition levels to be processed.

Based on previous information and on each wavelet basis characteristics, we decide to study how to select the set of decomposition levels that attain a good increase in the contrast, matching both quality measures and ROIs visual content. The following bases were chosen: the Daubechies 12 for calcifications, Symlets 12 for

cluster, Biorthogonal 2.2 for masses and Reverse Biorthogonal 1.3 for spiculated regions.

Then PCA was applied to the rotated data (See Section 4). Figures 13 and 14 shows the *loadings* corresponding to Daubechies 12 and Biorthogonal 2.2 bases. In Figure 13 meaningful differences are noticeable amongst three groups of combinations of decomposition levels: combinations on the first quadrant, combinations on the fourth quadrant and the rest of the combinations. The more pronounced differences (given by the almost orthogonality of the *loadings*) are shown in the combinations of the first and fourth quadrant. In Figure 14, a combination of levels remarkably distinguishes from the rest stands out.

Figure 15 shows the Manhattan plot for the selected bases according to *CEM* measure. It can be noticed that two principal components were enough in order to represent the whole data variability.

Applying the criterion for the “suitable” levels combination we get (3,6) for Daubechies 12 and Symlets 12, and (1,2,3,4) combinations for Biorthogonal 2.2 and Reverse Biorthogonal 1.3.

In Figure 16 we illustrate that the proposed algorithm with the selected bases and “suitable” levels combination is successful only for calcifications and masses.

7 Conclusions

Conventional contrast enhancement methods do not work properly in mammography images. The techniques based on wavelet transform have shown their capability for the detection of anomalies that can occur in the mammogram allowing the increase of its contrast.

The presented algorithm, LDWT with S-LIP model and modification of detail coefficients using Local Correlation method, has better results increasing the contrast of calcifications and masses, although it is able to improve the contrast of the rest of the anomalies. Values of the quality measures do not always correspond to the visual results because the process heavily depends on the choice of ROI and the measure of quality used.

As result of the experimentation performed the best wavelet bases were Daubechies 12 for

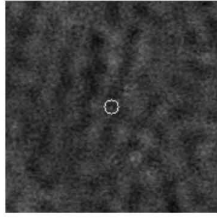
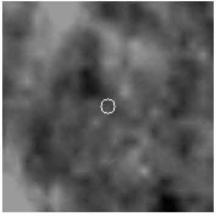
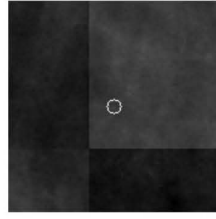
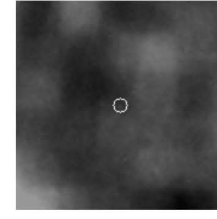
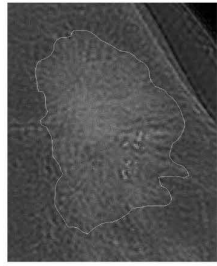


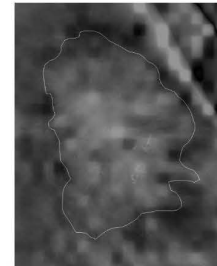
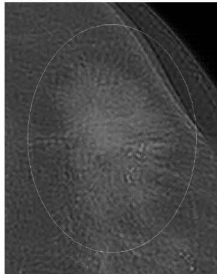

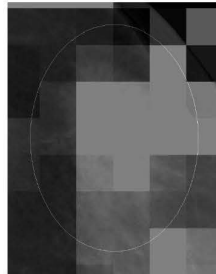
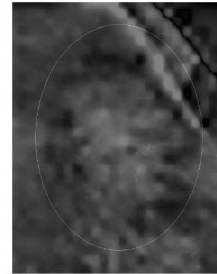
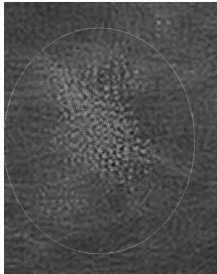
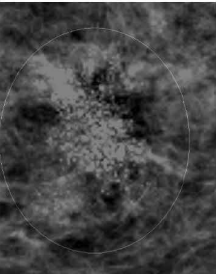
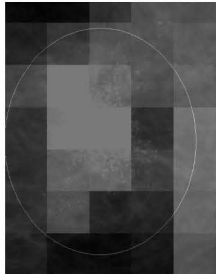
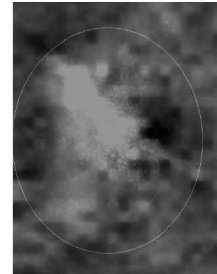
<i>CII</i>	Best base for Calcification dmey <i>Levels</i> = (1, 2, 4)	Best base for Mass bior2.2 <i>Levels</i> = (4, 5, 6, 7, 8)	Best base for Spiculated region bior1.1 <i>Levels</i> = (8, 9)	Best base for Cluster rbio1.3 <i>Levels</i> = (6, 8)
Calcification (ROI #57)				
	<i>CII</i> = 1.025 <i>CEM</i> = 3.626	<i>CII</i> = 1.028 <i>CEM</i> = 1.672	<i>CII</i> = 1.032 <i>CEM</i> = 2.78	<i>CII</i> = 1.029 <i>CEM</i> = 3.349
Mass (ROI #94)				
	<i>CII</i> = 1.545 <i>CEM</i> = 7.01	<i>CII</i> = 3.51 <i>CEM</i> = 28.311	<i>CII</i> = 3.092 <i>CEM</i> = 33.026	<i>CII</i> = 2.261 <i>CEM</i> = 13.506
Spiculated region (ROI #95)				
	<i>CII</i> = 1.236 <i>CEM</i> = 9.429	<i>CII</i> = 1.313 <i>CEM</i> = 11.458	<i>CII</i> = 1.457 <i>CEM</i> = 26.313	<i>CII</i> = 1.236 <i>CEM</i> = 9.402
Cluster (ROI #1)				
	<i>CII</i> = 1.115 <i>CEM</i> = 8.716	<i>CII</i> = 1.138 <i>CEM</i> = 9.178	<i>CII</i> = 1.257 <i>CEM</i> = 14.134	<i>CII</i> = 1.263 <i>CEM</i> = 13.107

Fig. 9. Best wavelet bases by type of anomalies according to *CII* measure

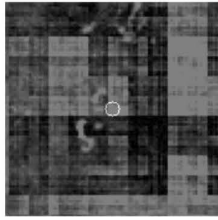
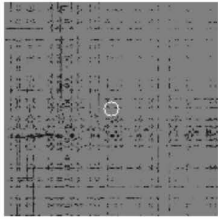
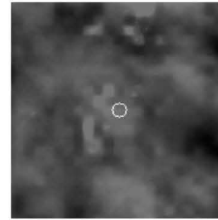
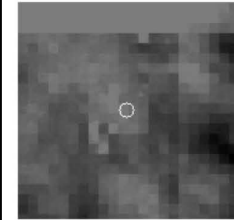
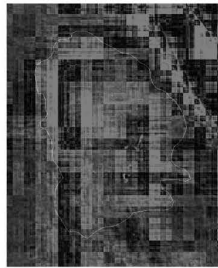

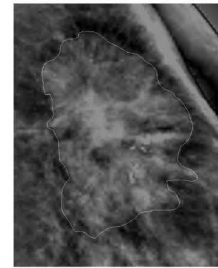
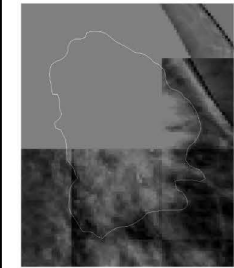
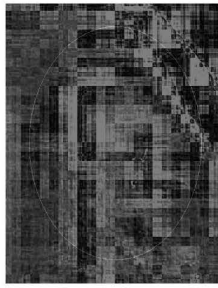
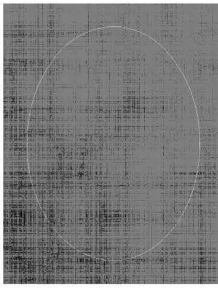
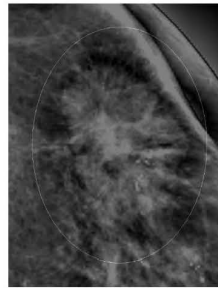
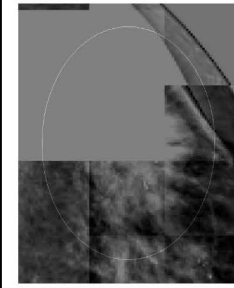
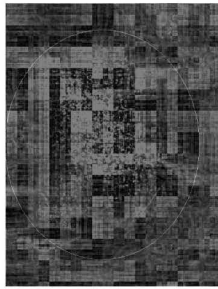
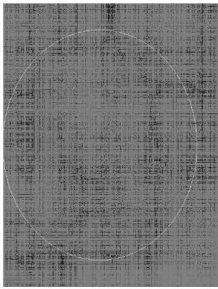
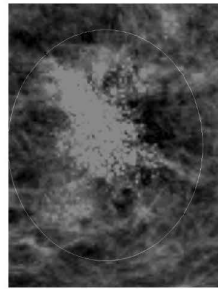
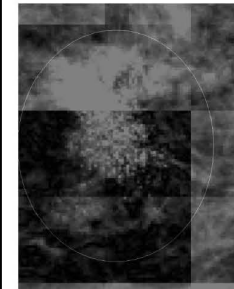
<i>CEM</i>	Best base for Calcification rbio3.3 <i>Levels = (2, 3, 4, 6, 7)</i>	Best base for Mass rbio3.1 <i>Levels = (2, 4, 8)</i>	Best base for Spiculated region rbio1.3 <i>Levels = (4, 5, 6, 7, 8)</i>	Best base for Cluster bior1.1 <i>Levels = (4, 5, 6, 7, 8, 10)</i>
Calcification (ROI #24)				
	<i>CII = 0.949 CEM = 1.332</i>	<i>CII = 0.987 CEM = 14.687</i>	<i>CII = 0.976 CEM = 48.421</i>	<i>CII = 0.978 CEM = 9.143</i>
Mass (ROI #94)				
	<i>CII = 1.774 CEM = 9.468</i>	<i>CII = 0.572 CEM = 1.576</i>	<i>CII = 2.261 CEM = 13.506</i>	<i>CII = 1.817 CEM = 16.414</i>
Spiculated region (ROI #95)				
	<i>CII = 1.08 CEM = 5.576</i>	<i>CII = 1.048 CEM = 29.957</i>	<i>CII = 0.939 CEM = 1.579</i>	<i>CII = 1.227 CEM = 24.056</i>
Cluster (ROI #1)				
	<i>CII = 1.085 CEM = 6.905</i>	<i>CII = 0.999 CEM = 28.336</i>	<i>CII = 1.24 CEM = 11.496</i>	<i>CII = 1.029 CEM = 2.728</i>

Fig. 10. Best wavelet bases by type of anomalies according to *CEM* measure

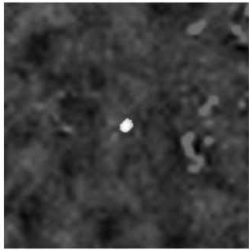
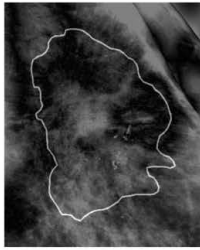
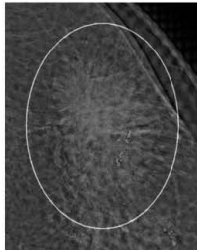
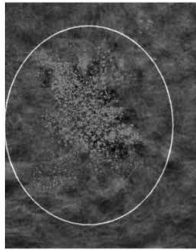
Calcification (ROI #36) sym9 Levels = (3, 4, 5)	Mass (ROI #94) bior3.1 Levels = (2, 4, 5, 6, 7, 8)	Spiculated region (ROI #95) db10 Levels = (3, 4, 5, 6)	Cluster (ROI #1) bior3.3 Levels = (3, 5, 6, 7)
			
$CIH = 0.989$ $CEM = 1.451$	$CIH = 0.264$ $CEM = 8.603$	$CIH = 1.22$ $CEM = 9.004$	$CIH = 1.117$ $CEM = 8.363$

Fig. 11. Some good visual results for each type of anomalies

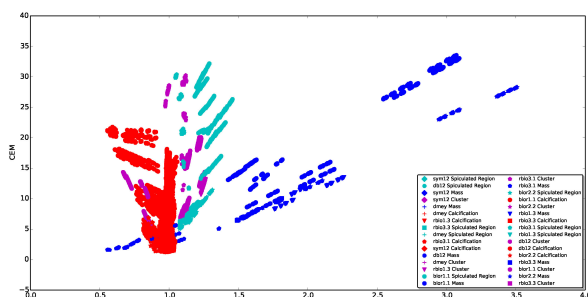


Fig. 12. Bivariate plot of CIH versus CEM

calcifications, Symlets 12 for cluster, Biorthogonal 2.2 for masses and Reverse Biorthogonal 1.3 for spiculated regions. Also, a methodology was proposed to select the combination of decomposition levels to be processed. This procedure consists of performing PCA on the data by taking the values of the CEM measure.

The variability of the data using Manhattan plots was studied and an algorithm was proposed to determine the "suitable" combination of levels. For the masses and calcifications the "suitable" combination was (3,6), and for cluster and spiculated region (1, 2, 3, 4) was obtained.

The ROI's definition is an important factor to explain the poor contrast improvement of the rest of the anomalies.

Acknowledgment

Authors thank the INbreast database courtesy of the Breast Research Group, INESC Porto, Portugal.

References

1. **Bhateja, V. & Devi, S.,** . Combination of wavelet analysis and non-linear enhancement function for computer aided detection of microcalcifications. *International Conference on Biomedical Engineering and Assistive Technologies (BEATS-2010)*, At Jalandhur (India).
2. **Bhateja, V., Misra, M., & Urooj, S. (2016).** Human visual system based unsharp masking for enhancement of mammographic images. *Journal of Computational Science*.
3. **Bradski, G. R. (2000).** The OpenCV Library. *Dr. Dobb's Journal of Software Tools*.
4. **Chen, L., Chen, C. W., & Parker, K. J. (1997).** Adaptive feature enhancement for mammographic images with wavelet multiresolution analysis. *Journal of Electronic Imaging*, Vol. 6, No. 4, pp. 467–478.
5. **Cheng, H., Min, R., & Zhang, M. (2010).** Automatic wavelet base selection and its application to contrast enhancement. *Signal Processing*, Vol. 90.
6. **Courbebaisse, G., Trunde, F., & Jourlin, M. (2002).** Wavelet Transform and LIP Model. *Image Analysis & Stereology*, Vol. 21, No. 2, pp. 121–125.

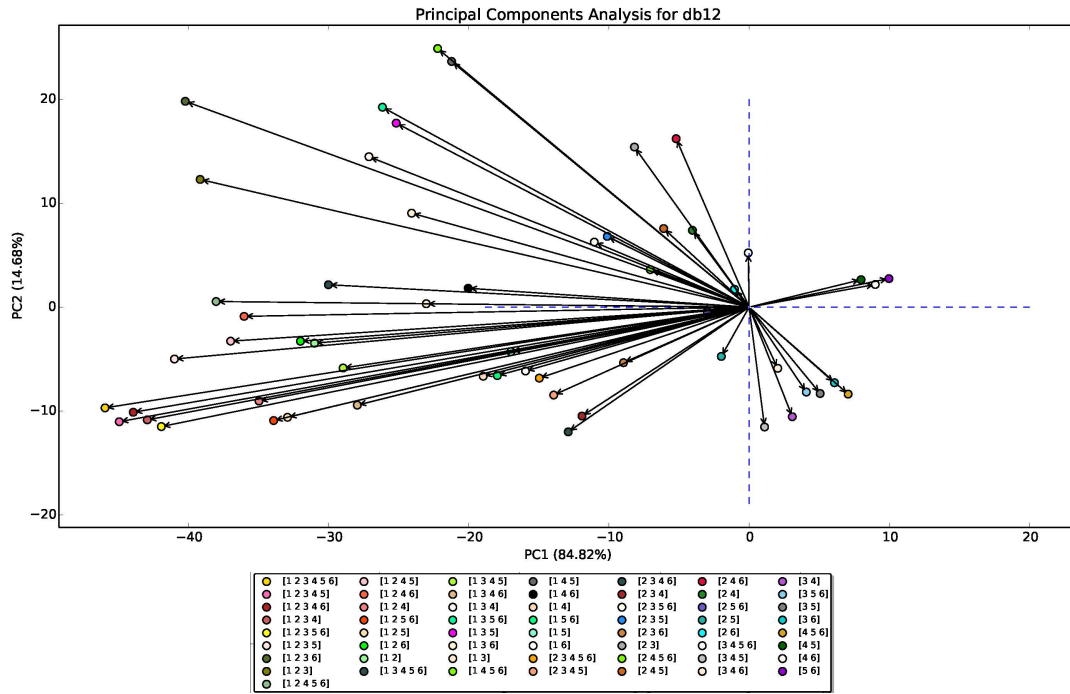


Fig. 13. Loadings of two principal components for data of Daubechies 12 wavelet base

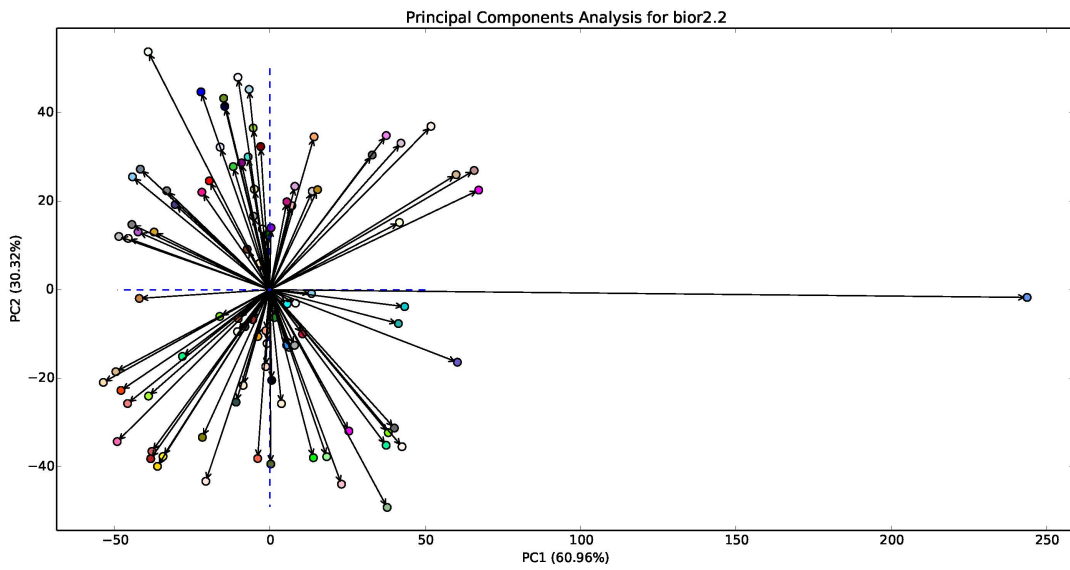


Fig. 14. Loadings of two principal components for data of Biorthogonal 2.2 wavelet base

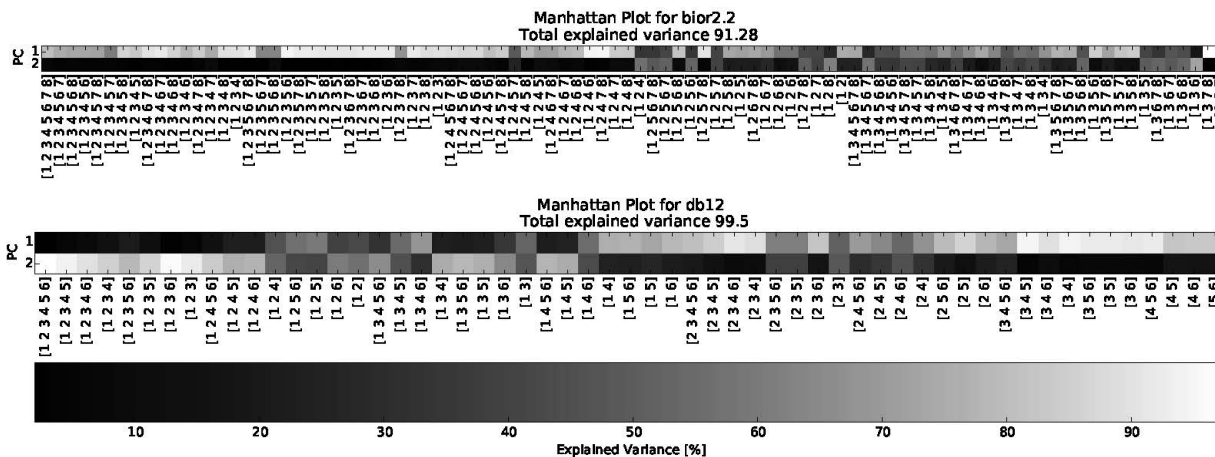


Fig. 15. Manhattan plots of CEM corresponding to PCA for selected wavelet bases

Calcification (ROI #36) db12 Levels = (3, 6)	Mass (ROI #94) bior2.2 Levels = (1, 2, 3, 4)	Spiculated region (ROI #95) rbio1.3 Levels = (1, 2, 3, 4)	Cluster (ROI #1) sym12 Levels = (3, 6)
CHI = 0.991 CEM = 1.7	CHI = 1.545 CEM = 6.995	CHI = 1.228 CEM = 9.186	CHI = 1.1 CEM = 7.969

Fig. 16. Results of the proposed algorithm for some ROIs according to the selected wavelet basis and combination of decomposition levels

7. Dahl, T., Tomic, O., Wold, J., & N, T. (2008). Some new tools for visualising multi-way sensory data. *Food Quality and Preference*, Vol. 19.

8. do Nascimento, M. Z., Martins, A. S., Neves, L. A., Ramos, R. P., Flores, E. L., &

Carrijo, G. A. (2013). Classification of masses in mammographic image using wavelet domain features and polynomial classifier. *Expert Systems with Applications*, Vol. 40.

9. Drukker, K., Malkov, S., Avila, J., Kerlikowske,

- K., Joe, B., Krings, G., Creasman, J., Drukteinis, J. S., Pereira, M. M., Kazemi, L., Shepherd, J., & Giger, M. (2016). Identification, segmentation, and characterization of microcalcifications on mammography. **Tourassi, G. D. & Armato, S. G.**, editors, *SPIE Proceedings Medical Imaging 2016: Computer-Aided Diagnosis*, volume 9785, San Diego, California, United States.
10. **Florea, C. (2009)**. Non-linear Image Representation and Pixel-wise Processing for Enhancing Images Acquired with Digital Cameras. *University "Politehnica" of Bucurest, Faculty of Electronics Telecommunication and Information Technology*.
 11. **Gao, R. X. & Yan, R. (2010)**. *Wavelets: Theory and Applications for Manufacturing*. Springer.
 12. **Gonzalez, R. C., Woods, R. E., & Eddins, S. L. (2009)**. *Digital Image Processing Using MATLAB*. Gatesmark Publishing, 2nd edition.
 13. **Gupta, R., Bhateja, V., et al. (2012)**. A log-ratio based unsharp masking (um) approach for enhancement of digital mammograms. *Proceedings of the CUBE International Information Technology Conference*, ACM, pp. 26–31.
 14. **Hunter, J. D. (2007)**. Matplotlib: A 2D Graphics Environment. *Computing in Science and Engineering*, Vol. 9, No. 3, pp. 90–95.
 15. **Jolliffe, I. (2010)**. *Principal Component Analysis*. Springer Series in Statistics. Springer, 2nd edition.
 16. **Jones, E., Oliphant, T., & Peterson, P. (2014)**. *Scipy: Open Source Scientific Tools for Python*.
 17. **Jourlin, M. (2016)**. *Logarithmic Image Processing: Theory and Applications*. Advances in Imaging and Electron Physics 195. Academic Press.
 18. **Kopans, D. B. (2006)**. *Breast Imaging*. Lippincott Williams & Wilkins, 3rd edition.
 19. **Laine, A. F., Fan, J., & Yang, W. (1995)**. Wavelets for Contrast Enhancement of Digital Mammography. *IEEE Engineering in Medicine and Biology Magazine*, Vol. 14, No. 5, pp. 536–550.
 20. **Laine, A. F. & Song, S. (1992)**. Multiscale Wavelet Representations for Mammographic Feature Analysis. *San Diego'92*, International Society for Optics and Photonics, pp. 306–316.
 21. **Mallat, S. G. (2009)**. *A wavelet tour of signal processing: the sparse way*. Elsevier/Academic Press, Amsterdam ; Boston, 3rd edition.
 22. **Martins, N., Pereira, C., & Ferreira, M. (2014)**. Digital Mammograms Contrast Enhancement using Wavelets – A Comparative Study. *IEEE International Symposium on Medical Measurements and Applications (MeMeA)*, IEEE, pp. 1–6.
 23. **Moreira, I. C., Amaral, I., Domingues, I., Cardoso, A., Cardoso, M. J. a., & Cardoso, J. S. (2012)**. INbreast: Toward a Full-field Digital Mammographic Database. *Academic Radiology*, Vol. 19, No. 2, pp. 236–248.
 24. **Mudigonda, N., Rangayyan, R., & Leo Desautels, J. (2001)**. Detection of breast masses in mammograms by density slicing and texture flow-field analysis. *IEEE Transactions on Medical Imaging*, Vol. 20.
 25. **Navarro, L., Courbebaisse, G., & Jourlin, M. (2014)**. Logarithmic Wavelets. In *Advances in Imaging and Electron Physics*, volume 183. Elsevier, pp. 41–98.
 26. **Navarro, L., Deng, G., & Courbebaisse, G. (2013)**. The Symmetric Logarithmic Image Processing Model. *Digital Signal Processing*, Vol. 23, No. 5, pp. 1337–1343.
 27. **Pedregosa, F., Varoquaux, G., Gramfort, A., Michel, V., Thirion, B., Grisel, O., Blondel, M., Prettenhofer, P., Weiss, R., Dubourg, V., Vanderplas, J., Passos, A., Cournapeau, D., Brucher, M., Perrot, M., & Duchesnay, E. (2011)**. Scikit-learn: Machine learning in Python. *Journal of Machine Learning Research*, Vol. 12, pp. 2825–2830.
 28. **Provenzi, E. & Caselles, V. (2014)**. A wavelet perspective on variational perceptually-inspired color enhancement. *International Journal of Computer Vision*, Vol. 106.
 29. **Rafiee, J., Tse, P., Harifi, A., & Sadeghi, M. (2009)**. A novel technique for selecting mother wavelet function using an intelligent fault diagnosis system. *Expert Systems with Applications*, Vol. 36, No. 3, pp. 4862–4875.
 30. **Rangayyan, R. M. (2004)**. *Biomedical Image Analysis*. CRC Press.
 31. **Risvik, H. (2008)**. *Visualizing Multi-Way Sensory Data*. Master's thesis, University of Oslo, Norway.
 32. **Sakellaropoulos, G., Costaridou, E., & Panayiotakis, G. (2003)**. A Wavelet-based Spatially Adaptive Method for Mammographic Contrast Enhancement. *Physics in Medicine and Biology*, Vol. 48, No. 6, pp. 787.
 33. **Schebesch, F., Unberath, M., Andersen, I., & Maier, A. (2016)**. *Breast Density Assessment Using*

- Wavelet Features on Mammograms*. Springer Berlin Heidelberg, Berlin, Heidelberg, pp. 38–43.
34. **Singh, S. & Bovis, K. (2005)**. An Evaluation of Contrast Enhancement Techniques for Mammographic Breast Masses. *IEEE Transactions on Information Technology in Biomedicine*, Vol. 9, No. 1, pp. 109–119.
 35. **Stefanou, H., Kakouros, S., Cavouras, D., & Wallace, M. (2005)**. Wavelet-based Mammographic Enhancement. *Proc. of the Fifth Int. Netw. Conf. (INC)*.
 36. **Stewart, B. W. & Wild, C. P. (2014)**. *World Cancer Report 2014*. International Agency for Research on Cancer/World Health Organization, Lyon.
 37. **Valdés, D. (2015)**. Logarithmic Wavelets for Contrast Enhancement in Digital Mammography, Computer Science's Diploma Thesis, Faculty of Mathematics and Computer Science, Univeristy of Havana. Unpublished thesis.
 38. **van der Walt, S., Schönberger, J. L., Nunez-Iglesias, J., Boulogne, F., Warner, J. D., Yager, N., Gouillart, E., Yu, T., & the scikit-image contributors (2014)**. scikit-image: Image Processing in Python. *PeerJ*, Vol. 2, pp. 453.
 39. **van Rossum, G. (1995)**. Python Tutorial. Technical Report CS-R9526, Centrum voor Wiskunde & Informatica (CWI), Amsterdam.
 40. **Vikhe, P. S. & Thool, V. R. (2016)**. Mass detection in mammographic images using wavelet processing and adaptive threshold technique. *Journal of Medical Systems*, Vol. 40.
 41. **Walt, S. v. d., Colbert, S. C., & Varoquaux, G. (2011)**. The NumPy Array: A Structure for Efficient Numerical Computation. *Computing in Science & Engineering*, Vol. 13, No. 2, pp. 22–30.
 42. **Wasilewski, F. (2006)**. Analysis and classification of medical signals using wavelet transforms.
 43. **Yan, Z., He, X., Liu, S., & Lu, D. (2001)**. An approximation-weighted detail contrast enhancement filter for lesion detection on mammograms. *Conference Proceedings of the 23rd Annual International Conference of the IEEE Engineering in Medicine and Biology Society*, volume 3, Istanbul, Turkey.

Article received on 14/02/2017; accepted on 20/09/2017.
Corresponding author is Damian Valdés Santiago.